

PVP2009-77522

## ANALYSIS OF SURFACE STRAINS AND LEAKAGE BEHAVIOR IN COMPOSITE PIPES AND VESSELS USING DIGITAL IMAGE CORRELATION TECHNIQUE

Renke Scheuer  
Institute of Materials Science  
An der Universität 2  
30823 Garbsen, Germany

Pierre Mertiny\*  
University of Alberta  
4-9 Mechanical Engineering Building  
Edmonton, Alberta, T6G 2G8, Canada

Dirk Bormann  
Institute of Materials Science  
An der Universität 2  
30823 Garbsen, Germany

### ABSTRACT

Pipe and vessel structures made from fiber-reinforced polymer composites are known to commonly outperform metallic structures in terms of corrosion resistance and strength-to-weight ratio. However, composite pressure piping and vessels without internal lining are prone to leakage failure caused by matrix cracking. Microscopic fractures in the often brittle matrix phase grow and coalesce under loading, forming a network of matrix cracks that facilitates fluid to permeate the pipe or vessel wall. Hence, liners are often incorporated into composite pressure containment structures. Leakage failures usually occur considerably below pressures causing rupture of composite pipes and vessels. Hence, more efficient designs may be obtained if liners could be avoided altogether. To achieve this goal a thorough understanding of the damage mechanisms leading to leakage failure is required.

Composite pressure piping and vessels are generally manufactured using filament winding or similar techniques. Resulting interwoven fiber architectures are generally considered to influence strain patterns and leakage behavior. Classical experimental methods are usually unable to verify this hypothesis, and therefore modeling techniques have largely been employed. In the present study, the effect of fiber architecture on surface strain patterns and the initiation of leakage were investigated experimentally using digital image correlation technique. Surface strain maps were produced for tubular filament-wound composite specimens subjected to combined internal pressure and axial traction. The findings of this study indicate that no distinct correlation exists between surface strain patterns and leakage initiation points.

**Keywords:** Fiber-reinforced composite polymer pipe; Digital image correlation technique; Strain measurement.

### INTRODUCTION

Fiber-reinforced polymer composite (FRPC) piping offers better performance in terms of corrosion resistance and strength-to-weight ratio than most metallic piping, and cost advantages may thus be realized employing FRPC pipe in various industrial applications. Filament winding is commonly employed for the manufacturing process. Using state-of-the-art manufacturing equipment this process can largely be automated, which makes FRPC pipe even more cost-competitive. Because of these characteristics, FRPC piping has become an attractive alternative to metallic pipe for many branches of industry.

Even though FRPC materials have been in industrial use for decades, an understanding of their failure behavior is still limited. To enhance this knowledge an investigation on internally pressurized pipe was conducted. Thus far the only indicators for a defective pipe are obvious failure modes such as rupture, buckling, collapse or leakage. The latter failure mode is due to microscopic fractures in the polymer matrix that develop, grow and coalesce to a network of cracks. The aim of this study is to assess whether there is a distinct correlation between winding patterns, strain distributions, and leakage initiation points. If a correlation can be found, composite pipe could be improved by selecting most suitable fiber architectures and reinforcing pipe in vulnerable areas during the production process. Thus this study might result in improved performance of FRPC pipes. Some preceding studies already attempted to establish a correlation between strains and leakage initiation points, but did not fully succeed due to insufficient spatial resolution [1]. Theoretical studies such as [2] used FEA to predict strains and leakage initiation points.

Considering that the phenomenon of matrix cracking is not limited to part of the specimen surface, a full-field strain measurement technique is required. As mentioned above,

---

\* Author to whom correspondence should be directed:  
Phone: 780-492-6982; Fax: 780-492-2200;  
Email: pmertiny@ualberta.ca

microscopic cracks usually grow and coalesce in the process of rising pipe stress to form a network of cracks, and hence, another attribute for a suitable measurement system is the ability to produce a detailed and time-dependent strain map. Digital Image Correlation (DIC) meets all these requirements, and thus was used for strain measurements in this study. Strain gages, which can only provide average values for highly localized areas, were used to validate DIC measurements. In the present paper, results from experiments with five different composite specimens are presented. Strain data obtained by DIC were evaluated and compared to filament winding patterns and leakage points that were also recorded by the image system.

## EXPERIMENTAL WORK

### Specimen Fabrication and Geometry

In this study an advanced E-glass was used (158B Type 30 by Owens Corning). Glass fiber rovings had a linear weight of 0.735 g/m. A Bisphenol-A epoxy system with a non-MDA polyamine hardener formed the polymer matrix (EPON826 with EPICURE9551 by Hexion Specialty Chemicals). Tubular specimens were produced by winding fiber materials onto chrome-plated steel mandrels. Eight E-glass strands were wound simultaneously forming winding bands with 5.88 g/m. A force of 27 N was applied to individual strands during winding using a numerical controlled tensioner. Specimens produced in this manner were given the designations B001, B002, B003 and B004. An additional specimen, B006, was produced using a narrower winding band with 2.94 g/m, which resulted in a fiber architecture with greater number of winding band undulations (for additional information on the winding process see e.g. [2]).

The diameter, free gage length and fiber architecture of all specimens was 38.1 mm, 90 mm and  $[\pm 45^\circ]_T$  respectively. The fiber volume fraction was determined as 65%; correspondingly, an effective wall thickness was determined as 0.58 mm. The effective wall thickness was calculated from the following information: applied winding angle, amount of deposited fiber material and fiber volume fraction [3]. This method gives a consistent measure for wall thickness since it neglects the resin rich layer on the outside of tubes that forms during manufacturing by excess resin accumulation. Depending on manufacturing conditions such resin-rich layers usually have considerable thickness variations.

### Speckle Pattern for DIC Analyses

Having a unique speckle pattern on the surface of each specimen was essential for the DIC method. The pattern was applied over a rectangular zone with axial orientation and dimensions 38.1 mm by 50.8 mm using ordinary white and black spray paint. Once a white base coat was completed, black paint dots with diameters ranging from 30  $\mu\text{m}$  and 250  $\mu\text{m}$  were applied. This corresponded to dot sizes, as observed by the CCD camera, with diameters between 1 and 7 pixels, which was an excellent dot size for DIC analyses. Prior to preparing the

speckle pattern strain gages were attached on the specimen surface in opposite corners of the rectangular pattern zone. To suppress light reflections and glare, black adhesive tape was also attached to the specimen surface as needed. A specimen close-up with speckle pattern and strain gages is shown in Fig.1.

### Testing Equipment

A custom-made testing machine was used to apply axial force and internal pressure to the specimens. To properly mount specimens into the testing machine's gripping system and load train for the application of axial force (shown in Fig.2), specimens were equipped with metallic end tabs. Hydraulic oil from a pressure intensifier was supplied to the specimen. The testing machine used an analog controller system in combination with a personal computer running National Instruments' LabView software. Besides controlling internal pressure and axial force this system also performed data acquisition tasks. The following data were recorded: test time, internal pressure, axial load, circumferential gage strain, and axial gage strain.

For full-field strain measurements a DIC system by Correlated Solutions was used. It consisted of two AVT Pike F421b cameras, each with a resolution of 2048x2048 pixels. Both cameras were equipped with a Nikon F-mount 28-85mm zoom lens and were connected to a second personal computer via a 'FireWire' connection. To obtain exact correlation results, stable, non-vibrating camera positions needed to be ensured. In addition, it was found that for optimal results, both cameras needed to be focused on the specimen surface having an angle of 30° to 40° between their optical axes. Proper camera positioning was accomplished using a custom-made camera mount that was attached to the testing machine. The distance between lenses and specimen surface was about 15 cm.

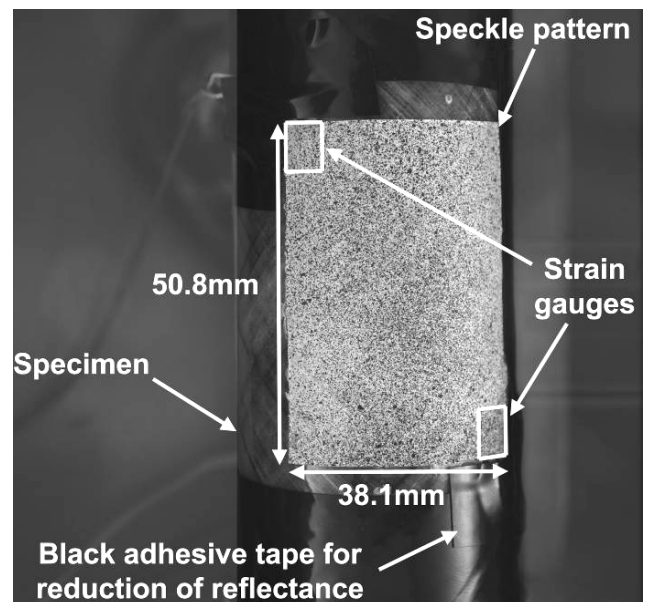


Figure 1: Specimen equipped with strain gages and speckle pattern.

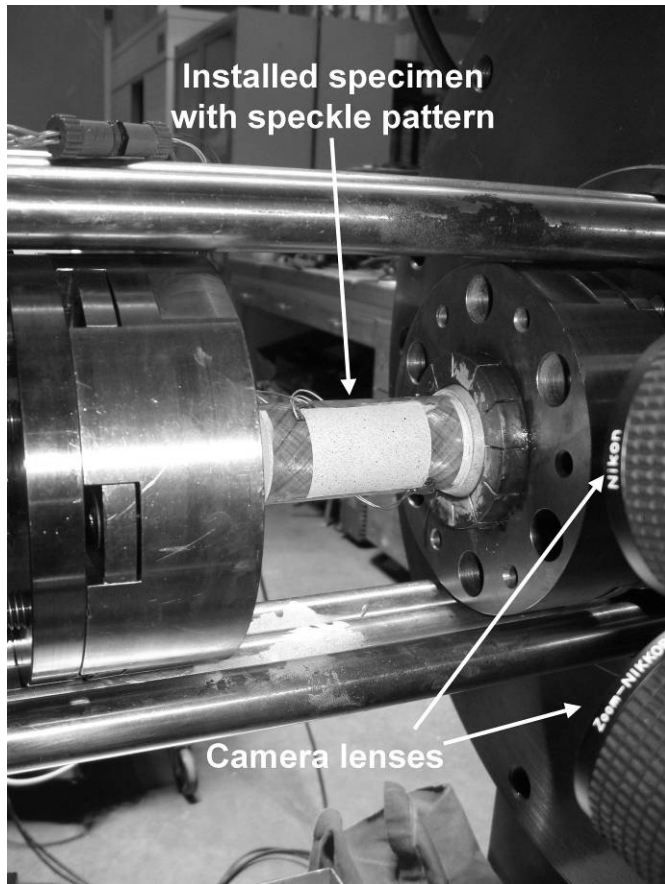


Figure 2: Specimen installed into testing machine.

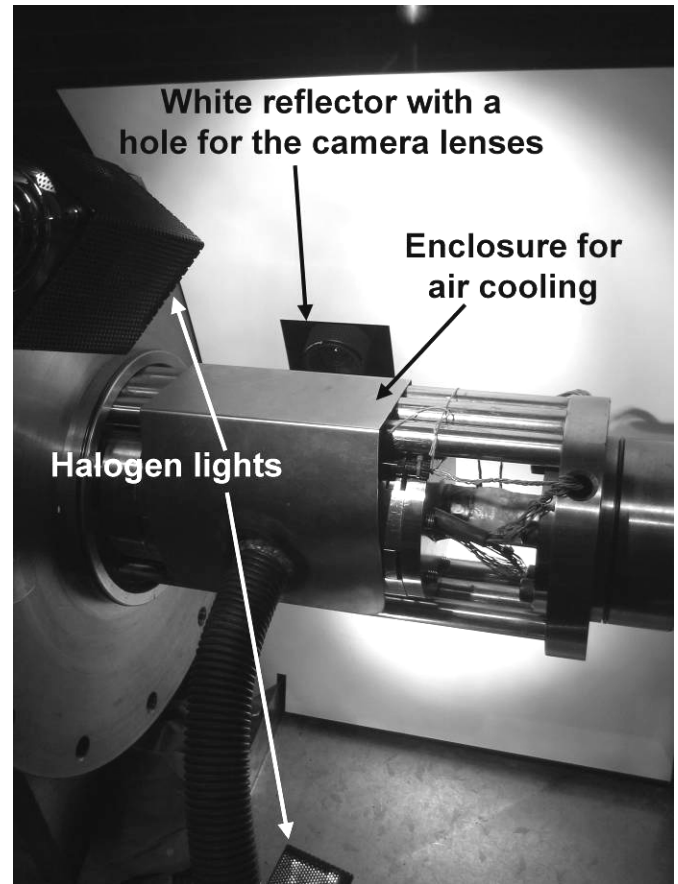


Figure 3: Final setup for DIC image acquisition.

Bright illumination of the specimen surface was required. To achieve even illumination without glare, a curved white reflector was used that was illuminated by two 250 W halogen lights, see Fig.3. To avoid thermal effects during testing, an ambient airstream was directed through a special enclosure onto the backside of the specimen. Once a steady state was reached the specimen temperature was 29°C, which was considered to be room temperature conditions.

### Experimental Procedures

Testing commenced once a specimen was properly installed, and setup and calibration of the DIC system were completed. Specimens were subjected to axial load and internal pressure resulting in a biaxial stress ratio  $\sigma_H/\sigma_A$  in the pipe wall of 1H/1A (i.e. equi-biaxial loading). Internal pressure was raised at a rate of 2.35 kPa/s. Note that only one specific loading rate was applied, and hence, time-dependent effects on damage were not investigated in this study. Axial force was adjusted by the controller system to maintain the specific stress ratio. To prevent pipe bursting, loading was terminated when a specimen pressure of 6.9 MPa was reached (i.e. the expected burst pressure), or when the pipe was completely covered with oil escaping from matrix cracks. Note that the DIC procedure was unable to process images as soon as oil drops appeared on the

specimen surface. Nevertheless, images were recorded for the entire test duration to allow for the determination of leakage initiation sites. Note that since the specimen changed length and diameter during testing, the locations of leakage sites needed to be related to specific speckles and not to image pixel locations.

### RESULTS

Testing showed that none of the FRPC specimens failed due to burst, and all specimens started to leak at a specific pressure. Leakage for B001 to B004 initiated at internal pressures between 3.5 MPa and 4.0 MPa while B006 started to leak earlier at a pressure of 2.5 MPa. Four to ten leakage initiation points appeared in the form of small oil drops on the surface of specimens that were produced with the wide winding band (B001 to B004). For B006, i.e. the specimen produced with the narrow winding band, six leakage initiation sites were observed that appeared in the form of lines rather than dots.

For each test a few thousand images were produced and used for post-processing to obtain high-accuracy maps for strains in circumferential and axial direction. To simply illustrate the development of strains, the number of images can generally drastically be reduced. In the present paper images are shown that were taken just prior to leakage obscuring the specimen surface (Figs.4-9). Also, observed leakage initiation

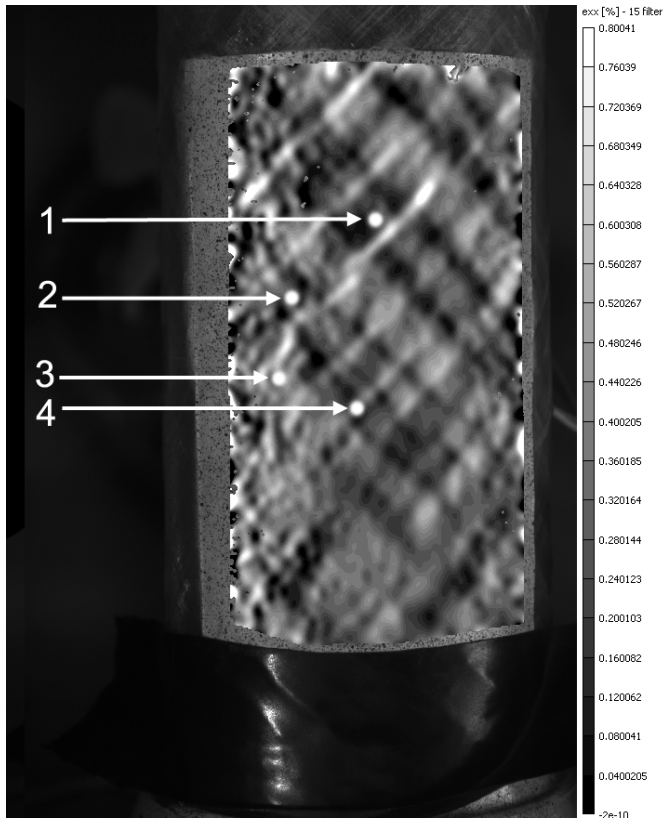


Figure 4: Map of hoop strain ('exx') for specimen B001.

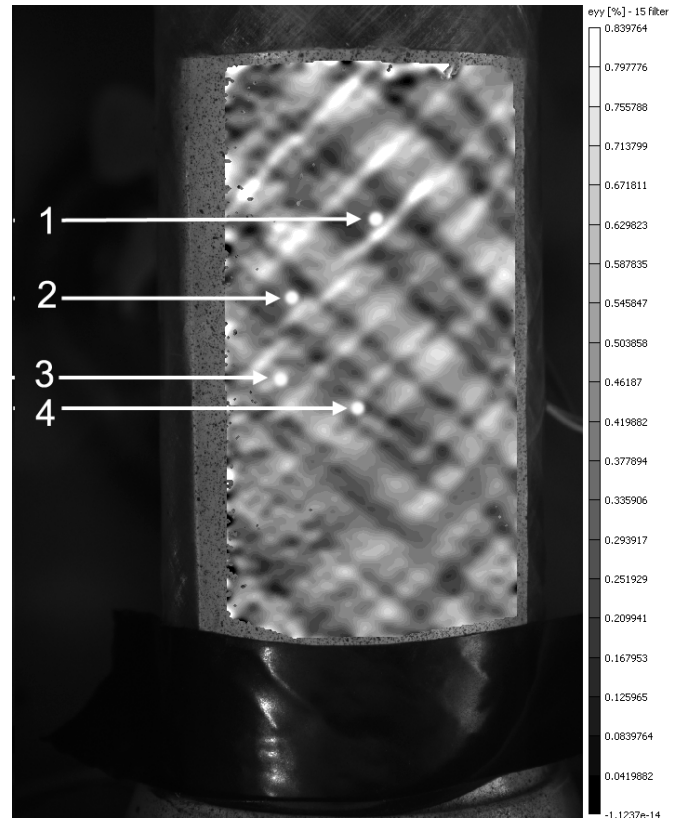


Figure 5: Map of axial strain ('eyy') for specimen B001.

sites were marked in these images by white dots or dashed lines to reveal any possible connections between strain patterns and leakage initiations sites. Another interesting detail is shown in the images for specimens B003, B004 and B006 (Figs.7-9). These specimens were wound with colored glass-fiber tracer threads that marked each side of the winding band. Hence, the winding band pattern could be reproduced and drawn onto the strain maps using white and grey lines. Note that parallel white and grey lines that are in close proximity to each other indicate a small winding band overlap that was adjusted to ensure full mandrel coverage and avoid any spots with weak or missing fiber reinforcement.

Correlated Solution's VIC-3D software was employed for image post-processing. Simply speaking, the DIC method measures deformation on an object surface by tracking gray scale patterns of small subsets of the full-field image. Using a standard deviation test, best correlation results were achieved with a subset size of 17 by 17 pixels. Such a subset included three to five pattern dots. Computing time and the size of output files vary inversely with the square of the step size (i.e. the location of the next subset). Optimum results with high accuracy and reasonable computing time were achieved for a step size of 4 pixels. Note that DIC results showed unreasonably high strain gradients at the fringes of the speckle pattern; hence, these areas were excluded from any analysis. Strain data within the area of interest, on the other hand, were

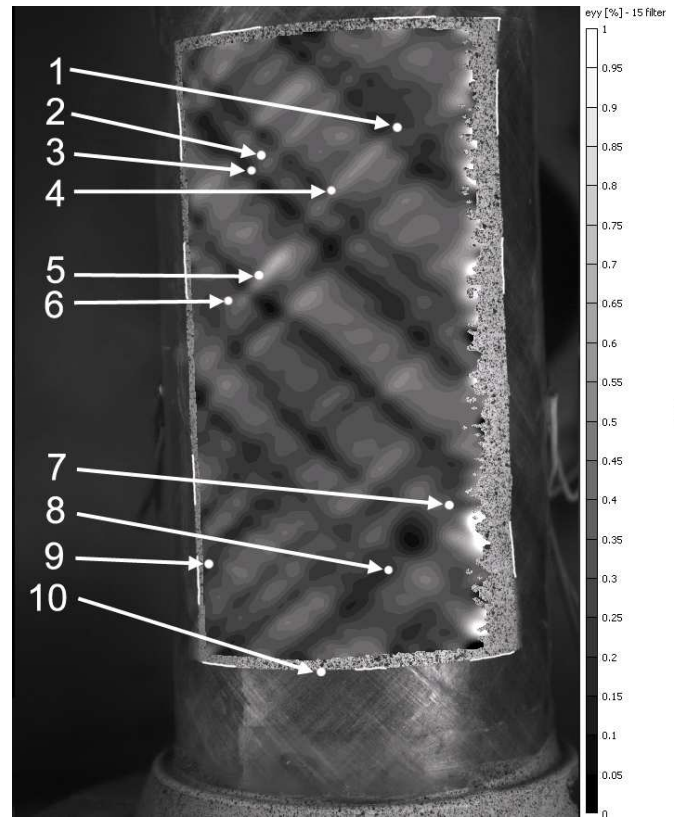


Figure 6: Map of axial strain ('eyy') for specimen B002.

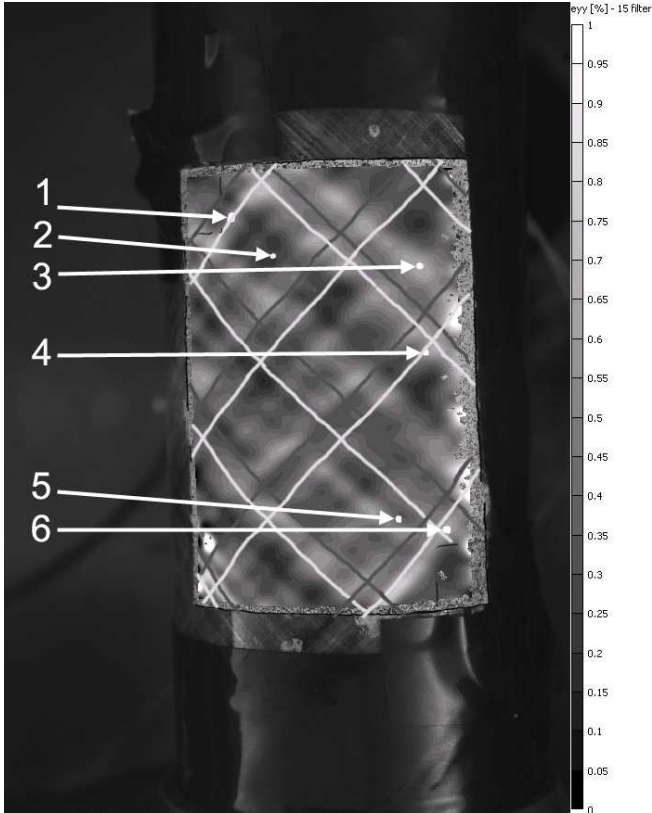


Figure 7: Map of axial strain ('eyy') for specimen B003.

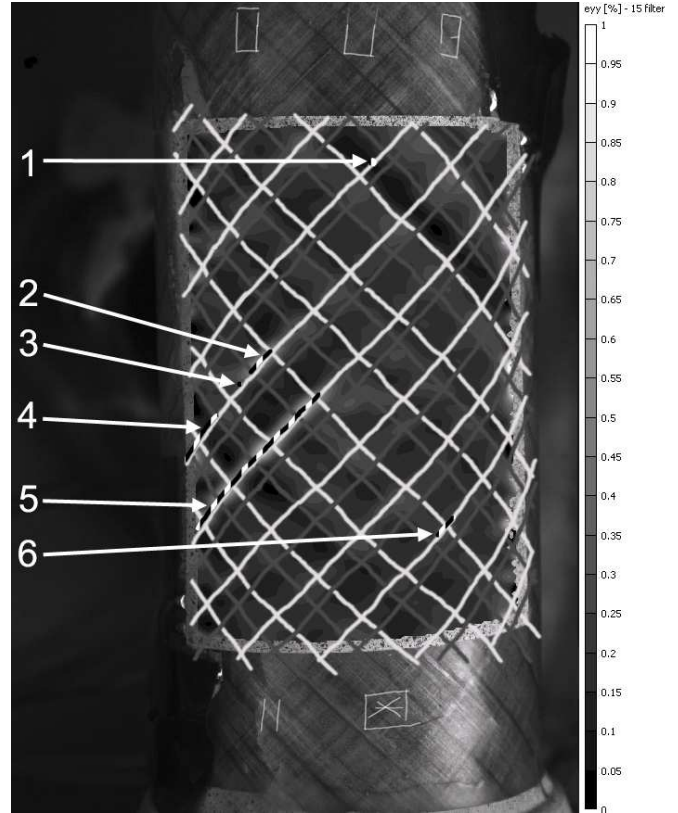


Figure 9: Map of axial strain ('eyy') for specimen B006.

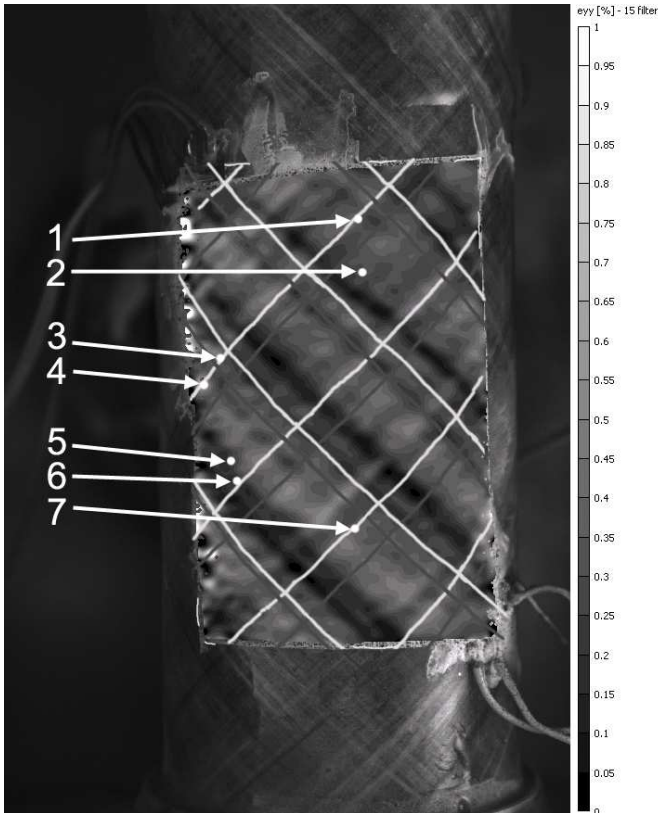


Figure 8: Map of axial strain ('eyy') for specimen B004.

highly accurate and repeatable; strain maxima varied only by an absolute 0.00145% between images taken of unloaded specimens. This small error, which is considered to have negligible effects on the analyses, is thought to be caused by floating point noise.

From hoop and axial strain maps shown in Figs.4 and 5 respectively, it can be observed that hoop strains had lower maxima (shown by the gray-scale bars) and were also lower on average (overall darker hoop strain map) than axial strains. This behavior was noticed for all specimens, i.e. average axial strain was approximately 20-30% higher than hoop strain. This can clearly be observed from load-strain plots like the one presented in Fig.10, which shows hoop and axial strains for specimen B002. This figure also indicates that strain gage data and DIC measurements were generally in good agreement.

### DISCUSSION

Present experiments showed that DIC is a reliable contactless method for measuring surface strains on composite specimens. Area averaged strains from DIC analyses that were produced for the five different FRP specimens agreed well with strain gage readings.

Axial strains were observed to be somewhat higher than circumferential strains. This trend was observed for all specimens. Equal strains in both directions were expected since specimens had 45° winding angles (causing orthotropic

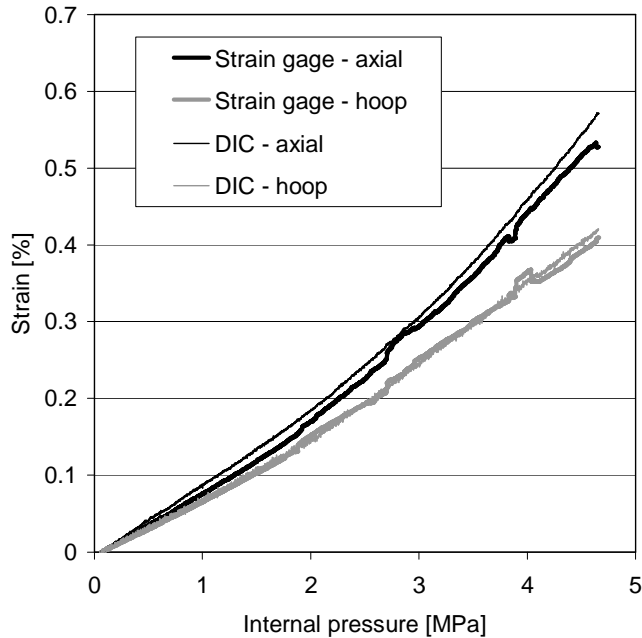


**Figure 10: Strain data from strain gages and area-averaged DIC measurements for specimen B002.**

properties) and were subjected to a stress ratio of 1H/1A (the exact stress ratio was 0.98 based on recorded force and pressure data and the effective wall thickness of 0.58 mm). One may speculate that small deviations in winding angle or residual stresses within the FRPC material may have caused the dissimilarities between hoop and axial strains; however, no conclusive explanation could yet be found for this phenomenon.

For all specimens made with the broad winding band, leakage initiation sites appeared in the form of dots. The number of dots within the area of interest varied from 4 to 10. No apparent correlation between strain intensities and locations of leakage initiation points could be ascertained. For example, leakage points #1 and #3 on specimen B002 were in zones of low strains while point #5 was in an area of a high strain (see Fig.6). Similar observation can be made for the other specimens.

Some degree of pattern regularity can be observed in the strain maps shown in Figs.4-8, in which zones of high and low strains are generally aligned with the 45° winding pattern. But this must be seen as a generalization since considerable strain variations still exist along the fiber direction. Also, zones of high and low strains do not consistently match up with the winding band patterns; it appears that with respect to winding band positions these zones were shifted for each specimen differently (see e.g. Figs.7 and 8).

In terms of leakage initiation sites, one may argue that specimen B002 exhibits three specific lines that include the majority of leakage points (see Fig.6). The first of these lines is defined by points #2 and #3; the second line by points #1, #4, #5 and #6; and the last line by the points #7, #8 and #10. Hence, the assumption could be made that these lines are

related to the location of winding bands. But, close investigation of strain maps containing sketches of the winding band pattern, e.g. for specimen B003 shown in Fig.8, refutes this assumption. Here leakage points appear in seemingly random positions in zones with strains of varying magnitude.

As mentioned above, the winding structure for specimen B006 is more interwoven and complex since this two-layer fiber architecture was produced with a narrower winding band than the other specimens (Otherwise, the material system and testing conditions were identical for both specimen types.). This resulted in a strain map with relatively low strain variability (see Fig.9), which thus offered even less clues for a possible correlation between winding pattern and leakage behavior. At the same time a more uniform strain distribution did not produce higher leakage strength, i.e. leakage failure for specimen B006 occurred at an internal pressurization of 2.5 MPa compared to 3.5 to 4.0 MPa for the other specimens. Leakage initiation sites also appeared in the form of lines rather than points (Figure 11 provides a close-up view of such a leakage line). Leakage lines were generally visible even with the naked eye. Note that zones of elevated strain accompanied the leakage lines, and that leakage lines were located at the winding band boundaries. Hence, it seems that in specimen B006 a separation between winding bands rather than cracking within the bands themselves was the dominating mechanism for leakage failure. This is different from the damage mechanism for the other specimens where highly localized leakage sites were observed. A reason for differences in damage behavior may lie in the altered winding procedure; however, further research is required to fully understand this phenomenon.

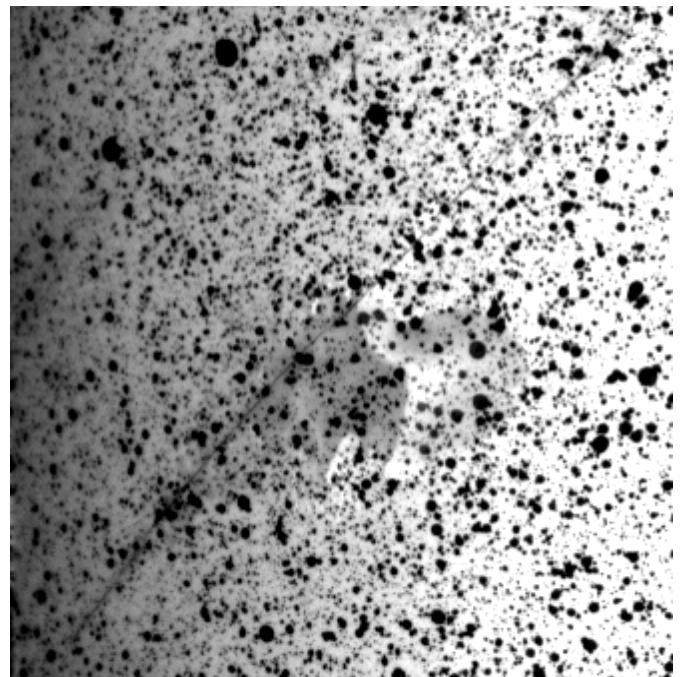


**Figure 11: Close-up view of leakage line #5 on specimen B006.**

Overall, the experiments showed that despite of a general correlation between strain and winding pattern, no apparent correlation between leakage initiation sites and surface strain patterns was evident for the present composite pipe specimens. Additional work is suggested to investigate the leakage phenomenon, using e.g. computerized tomography, to include information on density and matrix porosity distributions and wall thickness variations.

## CONCLUSIONS

In this paper results from an experimental study on fiber-reinforced polymer composite pipe structures were presented. Pipe samples with a two-layer [ $\pm 45^\circ$ ] fiber architecture were subjected to equi-biaxial loading caused by internal pressure and axial loading, and surface strain maps were produced using digital image correlation technique. Leakage initiation sites and winding band patterns were also considered in the analysis. The following conclusions were drawn from the experimental results:

- For all tests average strain in axial direction was higher than in hoop direction. Due to practically equi-biaxial loading conditions and orthotropic material properties, equal average axial and hoop strains were expected. The exact cause for the observed behavior is currently unknown.
- Leakage initiated between 3.5 MPa and 4.0 MPa internal pressure for specimens produced with a winding band of 5.88 g/m linear weight. Four to ten leakage initiation points were observed in the area captured for image analysis.
- A specimen produced with a winding band half the width of previous specimens (2.94 g/m), resulting in a more interwoven fiber architecture, leaked earlier at a pressure of 2.5 MPa. Six leakage initiation sites were observed that predominately appeared in the form of leakage lines (cracks) at winding band boundaries. This led to the conclusion that in this case, damage was largely caused by separation of winding bands.
- Positions of leakage initiation sites for all other specimens appeared to be of a random nature. No clear correlation between leakage points and surface strains or winding band pattern could be found.

- It is suggested to conduct further testing using additional methods like computerized tomography to find a possible correlation between leakage initiation sites and density/porosity distributions and/or wall thickness variations. Also, fatigue loading may be employed to promote accelerated crack formation and coalition, and thus possibly denser crack/leakage patterns, at lower biaxial stress levels than under monotonic loading conditions.

## ACKNOWLEDGEMENTS

This research project was made possible by the Dr.-Jürgen-Ulderup-Stiftung (Germany) as well as the Department of Mechanical Engineering at the University of Alberta, in particular the Advanced Composite Materials Engineering Group. The authors wish to acknowledge the financial and technical support of Syncrude Canada Ltd. and the Natural Sciences and Engineering Research Council (NSERC) of Canada. The authors would also like to extend thanks to Bernie Faulkner.

## REFERENCES

- [1] Juss, K., Kotlarski, J., Mertiny, P., 2007, "Detection of Matrix Cracking and Leakage in FRPC Tubes through Digital Image Analysis," Proc. 6th Canadian-International Composites Conference (Winnipeg, Manitoba), Aug. 2007.
- [2] Zhang, Y., Xia, Z., Ellyin, F., 2008, "Two-scale Analysis of a Filament-wound Cylindrical Structure and Application of Periodic Boundary Conditions". *Int. J. Solids and Structures* 45(20), pp. 5322-36.
- [3] Mertiny, P., Ellyin, F., 2002, "Influence of the Filament Winding Tension on Physical and Mechanical Properties of Reinforced Composites", *Composites A* 33(12), pp. 1615-22.